Probing Orientational Order of MHC Class I Protein and Lipids in Cell Membranes by Fluorescence Polarization-Resolved Microscopy Imaging

A. Kress, Patrick Ferrand, H. Rigneault, T. Trombik, H.-T. He, D. Marguet, S. Brasselet

Probing Orientational Behavior of MHC Class I Protein and Lipid Probes in Cell Membranes by Fluorescence Polarization-Resolved Imaging

Alla Kress,[†] Patrick Ferrand,[†] Hervé Rigneault,[†] Tomasz Trombik,[‡] Hai-Tao He,[‡] Didier Marguet,[‡] and Sophie Brasselet[†*]

[†]Aix-Marseille Université, Ecole Centrale Marseille, Centre National de la Recherche Scientifique, Institut Fresnel, Marseille, France; and [‡]Centre d'Immunologie de Marseille-Luminy, Institut National de la Santé et de la Recherche Médicale, Marseille, France, and Centre National de la Recherche Scientifique, Marseille, France

ABSTRACT Steady-state polarization-resolved fluorescence imaging is used to analyze the molecular orientational order behavior of rigidly labeled major histocompatibility complex class I (MHC I) proteins and lipid probes in cell membranes of living cells. These fluorescent probes report the orientational properties of proteins and their surrounding lipid environment. We present a statistical study of the molecular orientational order, modeled as the width of the angular distribution of the molecules, for the proteins in the cell endomembrane and plasma membrane, as well as for the lipid probes in the plasma membrane. We apply this methodology on cells after treatments affecting the actin and microtubule networks. We find in particular opposite orientational order changes of proteins and lipid probes in the plasma membrane as a response to the cytoskeleton disruption. This suggests that MHC I orientational order is governed by its interaction with the cytoskeleton, whereas the plasma membrane lipid order is governed by the local cell membrane morphology.

INTRODUCTION

Biomolecular orientational organization is a crucial factor in biological processes where functions can be closely related to orientation and ordering mechanisms. Proteins and lipids in cell membranes are known to form structured assemblies with collective molecular order participating in cell motility (1), vesicular trafficking (2), and signaling (3–5). Protein interactions in supramolecular complexes such as biofilaments are also highly driven by orientational order (6–8), which is crucial to study and understand the fundamental cell membrane mechanisms. Although biochemical investigations have proved to answer many important biological questions related to membranes, they fail in reporting location and orientational order of molecular entities because the spatial cell organization is lost in the cell lysis process. In contrast, fluorescence microscopy can handle such a task at the scale of the optical resolution.

Structural organization in cell membranes has been so far essentially studied in the frame of molecular spatial localization and its time dynamics. Fluorescence recovery after photobleaching (9), fluorescence correlation spectroscopy (10), and single molecule tracking (11) have allowed a better understanding of the mobility of proteins and lipids and their perturbation by specific conditions of the cells, bringing a considerable amount of information on the nanoscale organization of the cell membrane and its associated signaling dynamics. On the other hand, little attention has been directed toward protein and lipid orientational order in cell membranes.

Probing molecular orientation relies on the sensitivity of fluorescence to the coupling between optical polarization and molecular transition dipoles. Only a few works have reported investigations on biomolecules' orientational order in cell membranes, either from membrane proteins (12) or lipids (2,5,13–17), for two reasons:

First, polarization-resolved fluorescence imaging requires a fluorescent label rigidly attached to the system under study, able to report its orientational order behavior.

Second, the commonly used fluorescence anisotropy, based on the measurement of two polarization states in the excitation and detection paths, provides only partial information on the orientation of an ensemble of molecules (18,19).

Such a classical scheme quantifies molecular disorder only providing that the average orientation of these molecules is known. This has been limited so far to the investigations into simple spherical membranes geometries such as giant unilamellar vesicles (14), red blood cells (13,15), cell blebs (12), spherical cells (17,20), and nuclear envelopes (21).

Probing molecular orientational order in lipid membranes has been quite successful due to the possibility to rigidly embed fluorescent probes within the membrane leaflets. However, its application to the measurement of membrane proteins remains complex. Major histocompatibility complex class I (MHC I) has, nevertheless, been successfully labeled in a rigid way where a green fluorescent protein (GFP) is included within the transmembrane domain and the α3 extracellular domain of the MHC I protein (22). So far, the orientational order behavior of this system has been studied on round-shape cell blebs where the morphology of the membrane can be more easily analyzed (12).

In this article, we use a combination of fluorescence anisotropy and polarization-resolved fluorescence imaging

Submitted December 12, 2010, and accepted for publication May 11, 2011.

*Correspondence: sophie.brasselet@fresnel.fr

Editor: Michael Edidin.

0006-3495/11/07/0468/9 $2.00

doi: 10.1016/j.bpj.2011.05.021

(19,23), to quantitatively analyze the orientational order of MHC I on cell membranes in the endomembrane and plasma membrane. With this technique, we probe the angular range explored by the fluorescent labels (either GFP or lipid probe fluorophore) and explore how this angle can potentially report complementary information for the understanding of their biological function. The orientational order of MHC I in both membranes is expected to depend primarily on its lipid membrane environment, the maturation state of the protein, and its interaction with the cytoskeleton. In particular, MHC I is known to exhibit clustering in recognition processes (3,4), as well as hindered lateral mobility explained by dynamic barriers located in the cell cytoplasm (24,25). Such behaviors, which can lead to important consequences in its recognition functions (26,27), may be also related to modifications of the MHC I orientational order properties in the cell membranes.

In this work, the rigidly labeled MHC I is used to analyze its steady-state orientational order behavior. We report what we believe to be a first proof of principle of this technique by studying orientational order changes under actin and microtubule networks perturbations, induced by appropriate pharmacological treatments. Similar analysis performed on a lipid probe provides an additional picture of the molecular orientational order of the local lipid environment in the plasma membrane. The results show that molecular interactions with the cytoskeleton and cell membrane local morphology are determining factors in the proteins and lipids orientational order behaviors analyzed by polarization-resolved fluorescence imaging.

MATERIALS AND METHODS

Cell preparation

All experiments were carried out on COS-7 cells (ATCC No. CRL-1657; American Type Culture Collection, Manassas, VA). COS-7 cells were grown at 37°C in Lab-Tek chambers (Nalge Nunc, Rochester, NY) in DMEM medium (Lonza, Verviers, Belgium) completed by 10% FBS and 1% sodium pyruvate. The H2L^{d}GFPout and H2L^d GFPin molecular constructs are detailed in Marguet et al. (22), and are denoted MHC^{GFP}Rigid and MHC^{GFP}Flexible, respectively, for clarity throughout this article. A schematic of those two constructs are shown in Fig. 1, *a* and *b*. In MHC^{GFP}Rigid, the GFP probe is located within the amino-acid sequence of the H2L^d protein, which restricts its orientational degrees of freedom and makes it a rather rigid probe. In the case of MHC^{GFP}Flexible, GFP is attached to its cytoplasmic tail at the C-terminus, allowing mobility in large orientational angles (12).

Cells were transfected with MHC^{GFP}Rigid and MHC^{GFP}Flexible cDNA expression vector with ExGen 500 as per manufacturer's instructions (Euromedex, Souffelweyersheim, France) and 48 h before measurements. After this time, MHC I has migrated partly to the plasma membrane. Cells were washed and kept in Hanks buffered salt solution containing 10 mM HEPES (HBSS/HEPES), pH 7.4, at 37°C, for the whole imaging process (or 25°C for complements in the Supporting Material).

Cells were labeled with di-8-ANEPPQ directly before measurements. Cells were washed and incubated in insertion buffer (NaCl 130 mM, KCl 5 mM, $CaCl_2$ 10 mM, glucose 5 mM, and HEPES 10 mM) with 1 μM di-8-ANEPPQ (dissolved by absolute ethanol to 1 mM for preservation and usage) for 2 min at room temperature. After incubation, cells were washed again and kept in HBSS/HEPES at 37°C for the whole imaging process (or 25°C for complements in the Supporting Material).

For the pharmacological treatments, cells were washed in HBSS/HEPES and incubated at 37°C with 1 μM latrunculin A (5 min), or 10 μM cytochalasin D (30 min). Cells were then washed with HBSS/HEPES and kept in HBSS/HEPES with 10 times' diluted reagent during the whole imaging process. Cells were also incubated with 3 μM colcemid in DMEM medium for 5 h, washed, and imaged with HBSS/HEPES. At last, cells were swollen in a (80% H_2O, 20% HBSS/HEPES) solution and imaged after 15 min. All pharmacological treatments were performed after the transient transfection with MHC I and before di-8-ANEPPQ labeling.

Experimental setup

Experiments have been carried out on a custom laser scanning confocal microscope system (see Fig. S1 in the Supporting Material). The linearly polarized excitation beam from a continuous 491-nm laser (Calypso; Cobolt, Solna, Sweden) is reflected by a dichroic mirror (XF2037-500DRLP; Omega Optical, Brattleboro, VT) and focused on the sample

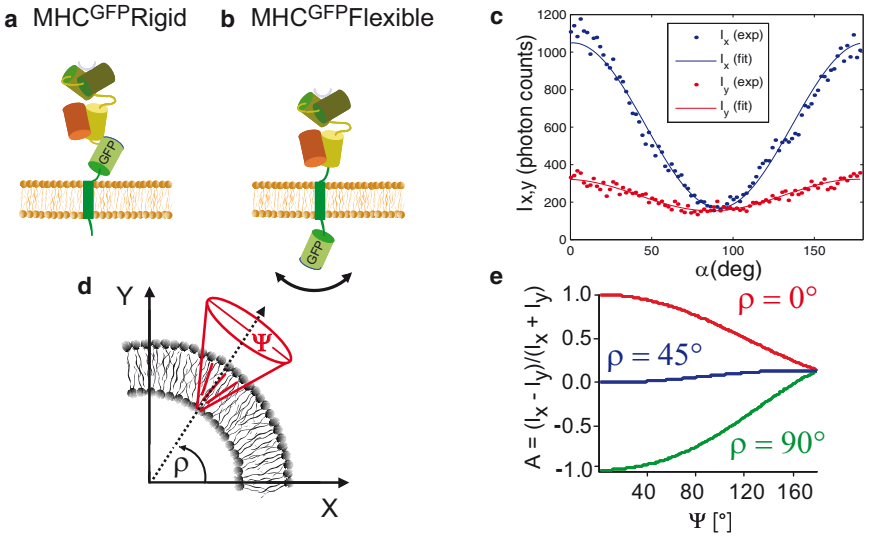

FIGURE 1 Schematic representation of (*a*) MHC^{GFP}Rigid and (*b*) MHC^{GFP}Flexible. (*c*) Typical polarimetry responses $I_X(\alpha)$ and $I_Y(\alpha)$ measured for a varying incident polarization angle α, at a given point of a di-8-ANEPPQ-labeled cell membrane. (*Continuous lines*) Fits (see the Supporting Material). (*d*) Scheme of a membrane equator representing the molecular orientational cone-shaped distribution with the cone aperture angle ψ of fluorescent probes inserted into the membrane or attached to a membrane protein. The *X* and *Y* axes define the sample plane in which the excitation polarization is fixed. The angle ρ specifies the cone orientation in this frame. (*e*) Anisotropy ratio $A(\psi)$ dependence for $\rho = 0°$ (*top line*), $\rho = 45°$ (*middle line*), and $\rho = 90°$ (*lower line*). This function accounts for polarization distortions in the setup (see text).

by a water immersion microscope objective (C-Apochromat 40× UV-VIS-NIR, NA = 1.2; Carl Zeiss, Aalen, Germany). The power at the entrance of the microscope is ~10–20 μW. The typical lateral optical resolution obtained is ~200 nm as characterized in Ferrand et al. (28). Fluorescence is collected by the same objective in an epi-geometry, passes through the dichroic mirror, and is spectrally filtered (HQ540/80M-2P; Chroma Technology, Rockingham, VT). After being focused in a confocal pinhole (75 μm diameter), the emission signal is split in two orthogonal polarization analysis directions (corresponding to the X and Y sample plane directions) by a polarizing beam splitter (broadband polarizing beamsplitter model No. 05FC16PB.3; Newport, Irvine, CA). The corresponding analyzed intensities I_X and I_Y are obtained by focusing the emitted signal onto two avalanche photodiodes (SPCM-AQR-14; PerkinElmer Optoelectronics, Waltham, MA).

Imaging is performed by scanning the excitation/observation volume in the sample, using galvanometric mirrors (28). For polarimetry imaging, the excitation polarization is linear in the sample plane (X,Y), rotated by an angle α with respect to the reference axis X. In this mode, α is controlled by a half-wave plate (WPH05M-488; Thorlabs, Newton, NJ) mounted on a motorized rotation stage (PR50CC; Newport), placed before the dichroic mirror. A stack of 90 images is recorded while α is incremented in 2° steps from 0° up to 180° for each scanning frame. A quantity of 150 × 150 pixels images is recorded on a 60 × 60 μm^2 sample area with a pixel dwell time of 100 μs for each angle α. The typical duration of acquisition for a polarimetry stack of 90 images is 5 min.

For each pixel of the image, polarimetric responses $I_X(\alpha)$ and $I_Y(\alpha)$ are generated (Fig. 1 *c*) and used either to get a direct molecular order information (see Methodology below), or to produce an anisotropy ratio image using the fact that the sum over all incident polarizations is equivalent to a circular excitation. Possible slight differences of efficiency between the two X and Y detectors are systematically assessed by comparing intensities measured in a 1-μM water solution of Rhodamine 6G, assumed to be isotropic, due to its fast molecular rotational dynamics. The obtained ratio $r = I_X/I_Y$ (typically between 0.85 and 0.9) is taken into account by rescaling the photon counts of the appropriate channel before data processing. Polarization distortions produced by the optics (in particular ellipticity and dichroism factor caused by the reflection on the dichroic mirror) are preliminarily characterized using a method developed in Schön et al. (29), based on polarimetry measurements in a 1-μM water solution of Rhodamine 6G, and systematically accounted for in the data analysis. At last, the high numerical aperture collection (NA = 1.2) is accounted for by introducing a degree of mixture of the I_X, I_Y, and I_Z emitted fluorescence signals along the X, Y, and Z polarization direction defined by the coefficients $K_1 = 0.86$, $K_2 = 0.015$, and $K_3 = 0.262$ with the notations of Axelrod (13).

Methodology

The polarization sensitivity of the fluorescence emitted by a collection of molecular dyes located in the focal volume of a microscope objective has been largely studied in both one-photon and two-photon excitation contrasts. Traditionally, molecular order in membranes, in a steady-state regime, is modeled by an angular cone aperture representing the directions explored by the probed molecules over a long time (typically 100 μs per pixel) comparing to orientational fluctuations (13,14). Assuming that the imaging plane is set at the equator of the membrane where the molecular cone distribution main axis lies in the (X,Y) sample plane, this cone is defined by its average orientation angle ρ relative to X and its aperture ψ (Fig. 1 *d*). Although this model is a crude simplification of the more general Boltzmann distribution, it has been shown to be robust enough to give a good representation of molecular orientational order (13). The fluorescence responses I_X and I_Y are modeled supposing that individual molecular absorption and emission dipoles lie within a cone distribution defined by (ρ,ψ) (19). The hypothesis of parallel absorption and emission dipoles directions is discussed below. In a membrane the two parameters ρ and ψ have a strong influence on the measured fluorescence polarization response.

The value ψ is traditionally measured using fluorescence anisotropy imaging (13,14,17,20). In this work we define the anisotropy polarization ratio by $A = (I_X - I_Y)/(I_X + I_Y)$ under circular incident polarization, depicted in Fig. 1 *e* as a function of ψ for different values of ρ. This definition of A, which is adequate for the epi-fluorescence microscopy geometry, differs from the usual fluorescence anisotropy as performed in a cuvette. We describe below its characteristics.

In the case of high molecular order (small cone aperture angle ψ), A reaches extreme values of (+1) when the fluorescence dipoles lie along the X axis in the sample plane ($\rho = 0°$), and (−1) when they lie along Y ($\rho = 90°$). In case of low molecular order (isotropic distribution of the dipoles: $\psi \sim 180°$), the A value tends toward $A = 0.14$ whatever the value of ρ. This value slightly differs from the expected 0 value, due to the instrumental polarization distortions described in Experimental Setup. Fig. 1 *e* shows that the measurement of A can be used to determine the molecular order aperture angle ψ, as long as ρ is known. However, although A is a good reporter of ψ at extreme ρ-values ($\rho = 0°$ and 90°), no valuable information can be retrieved close to $\rho = 45°$, because the detected fluorescence along the X and Y directions are almost equivalent in this case. We therefore limit our analysis to the sample regions where ρ is close to 0°, leading to a large range of positive values of A, to compare cells in different situations with the best comparison accuracy. Identifying ρ within a cell membrane is achievable when working with circular-shaped membranes such as systematically done in previous works (12,13,17,20). It becomes less obvious when working with cell membranes that have complicated shapes. To make sure that $\rho \sim 90°$ in our investigated cells, a full polarization response is performed using the polarimetry imaging scheme (Fig. 1 *c* and the Supporting Material) (19).

With these tools we 1), securely find $\rho \sim 0°$ membrane locations with polarimetry imaging; and 2), perform anisotropy imaging to determine the corresponding ψ angle at these locations, in regions of interest of 1×1 pixel centered on a given membrane location. The distributions of the values of ψ determined in the areas of interest are depicted as histograms measured over populations of 5–10 different cells for which typically 10–25 regions are measured, leading to 200 explored regions in total. In each case, the average ψ-values and their standard deviation are given. The standard deviation sums up intrinsic experimental noise, cell membrane, and cell-cell heterogeneities.

Photobleaching does not contribute to anisotropy measurements, because each pixel is illuminated for a short time (100 μs) in 90 successive images at a rate of roughly three images per second. Long time photobleaching, observed in our systems at timescales of up to 20 min under continuous illumination, is therefore not a limitation in this method (Fig. 1 *c*). In the our signal conditions, a bleaching by 7% of the measured intensity would induce a bias of ψ of roughly 10°, which is close to the measured standard deviations. At last, the measured ψ-values are representative of the population of proteins or lipids averaged in the focal volume, therefore, as for classical anisotropy, this method cannot discriminate monomeric versus polymeric states of proteins if the number of observed proteins is not a priori known.

Finally, anisotropy imaging permits a distinct visualization of the endomembrane and plasma membrane locations, which can be better discriminated from the isotropic population of proteins present in the cytoplasm. In all analyses, studies are performed on cells where a clear distinction can be made between the endomembrane and the plasma membrane.

RESULTS

Fig. 2 shows experimental anisotropy and fluorescence intensity images given by $I_X + I_Y$, summed over all incident polarization angles α.

Orientational order behavior of MHC I

Studies on the molecular order of membrane proteins in living cells require a rigidly labeled fluorescent probe. Our

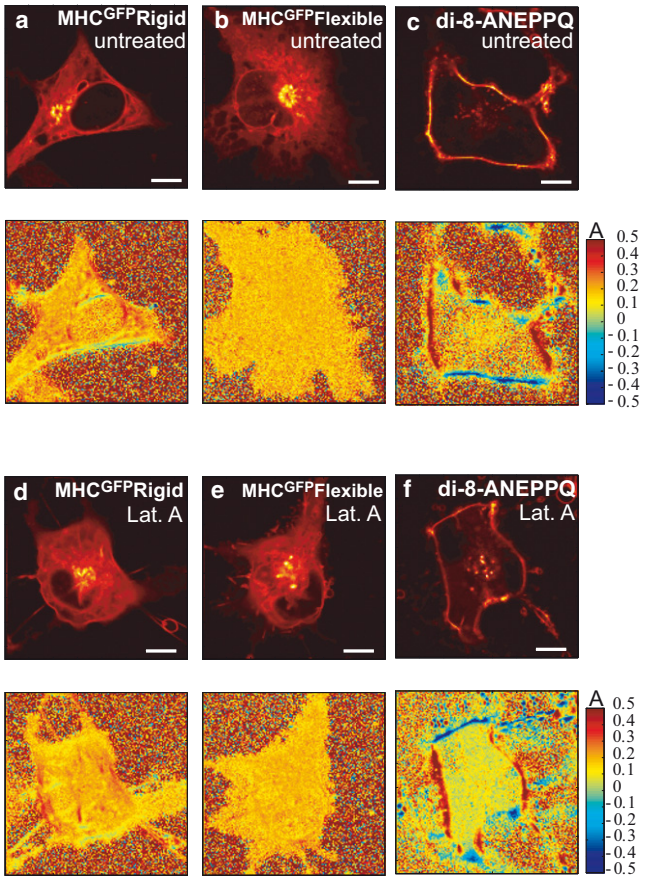

FIGURE 2 Fluorescence image (*top*) and corresponding anisotropy images (*bottom*) of COS-7 cells labeled with (*a*) MHC^{GFP}Rigid, (*b*) MHC^{GFP}Flexible, (*c*) di-8-ANEPPQ without treatments and (*d*) MHC^{GFP}Rigid, (*e*) MHC^{GFP}Flexible, (*f*) di-8-ANEPPQ treated with latrunculin A. The typical fluorescence intensity varies between 200 and 500 K counts/s. Scale bar: 10 μm.

experiments make use of two kinds of label attachment schemes developed previously (22), denoted MHC^{GFP}Rigid and MHC^{GFP}Flexible (see Fig. 1, *a* and *b*, and Materials and Methods). In the case of MHC^{GFP}Rigid, the GFP molecule is considered to be rather rigidly attached to the protein structure. As a control, in MHC^{GFP}Flexible, the GFP is considered flexible (12). In all analyses below, the absorption and emission angle of the fluorescence dipoles are supposed to lie along the same direction. This is supported by a previous analysis showing a 3° difference between these dipoles (12).

As can be seen in Fig. 2 *a*, COS-7 cells transfected with the MHC^{GFP}Rigid construct show large values of A in the endomembrane and the plasma membrane. This is a signature of a nonnegligible orientational order ($\psi < 180°$) of the proteins, for which we find a cone aperture angle ψ of ($158° \pm 6°$) in the endomembrane and ($148° \pm 9°$) in the plasma membrane. We do not observe values higher than $A = 0.5$, as compared to a complete order which would lead to $A = 1$. Contrary to MHC^{GFP}Rigid, the anisotropy image for MHC^{GFP}Flexible (Fig. 2 *b*) shows clear isotropic behavior of the label in endomembrane and plasma membrane of the cell. The A values measured are close to the theoretical isotropic value $A = 0.14$ is found, accounting for polarization distortions. Therefore the orientation of the protein cannot be accurately deduced and a large angle ψ of ($176° \pm 4°$) was measured whatever the membrane location, characteristic of an isotropic distribution of the molecules.

These results show that MHC^{GFP}Rigid confirms its ability to be a more sensitive label construct than MHC^{GFP}Flexible with respect to orientational order (12). We therefore extended the study to the influence of different reagents altering the state of actin and microtubules polymerization. The used reagents are latrunculin A (an actin polymerization inhibitor), cytochalasin D (an actin depolymerization inducer), and mechanical disruption of cytoskeleton by a hypotonic shock. Furthermore, we studied the influence of microtubules depolymerization by colcemid. The orientational order of MHC^{GFP}Rigid in the endomembrane and the plasma membrane is shown in the anisotropy images in Fig. 2 and the results are summarized in Table 1. In the case of MHC^{GFP}Flexible, an isotropic behavior was observed for all treatments (see the Supporting Material).

The swelling of the cells reveals a higher orientational order ($\psi = 146° \pm 8°$) in the endomembrane and higher orientational disorder ($\psi = 155° \pm 9°$) in the plasma membrane, as compared to the values reported for untreated cells. Latrunculin A and cytochalasin D are used to alter the state of actin polymerization by different mechanisms: Latrunculin A binds to actin monomers and prevents their polymerization whereas cytochalasin D binds the barbed-ends of the actin filaments and prevents the extension of actin filaments. Even though the overall effects of latrunculin A and cytochalasin D alter the actin-based cytoskeleton organization, we find different orientational behaviors on MHC^{GFP}Rigid.

Latrunculin A does not modify the orientational distribution of MHC^{GFP}Rigid in the endomembrane ($\psi = 156° \pm 8°$), but in the plasma membrane with a larger cone aperture angles ($\psi = 158° \pm 10°$). In the case of cytochalasin D treatment, the effect is less pronounced with no effect on the plasma membrane ($\psi = 148° \pm 8°$) but an orientational

TABLE 1 Summary of the obtained results for the cone aperture angles ψ, reporting the mean and standard deviation of ψ for the GFP-tagged MHC I proteins and the di-8-ANEPPQ lipid probes

	Endomembrane	Plasma	Plasma
COS-7 cells	MHC^{GFP}Rigid	MHC^{GFP}Rigid	di-8-ANEPPQ
Untreated	$158° \pm 6°$	$148° \pm 9°$	$132° \pm 12°$
Hypotonic shock	$146° \pm 8°$	$155° \pm 9°$	$98° \pm 10°$
Latrunculin A	$156° \pm 8°$	$158° \pm 10°$	$116° \pm 10°$
Cytochalasin D	$151° \pm 7°$	$148° \pm 8°$	$108° \pm 12°$
Colcemid	$147° \pm 8°$	$150° \pm 9°$	$117° \pm 11°$

distribution more ordered in the endomembrane ($\psi = 151° \pm 7°$). Finally colcemid, which depolymerizes the microtubules, leads to an increase of order in the endomembrane with $\psi = 147° \pm 8°$ and slight increase of disorder ($\psi = 150° \pm 9°$) in the plasma membrane. Altogether, these data suggest that disruption of the cytoskeleton/microtubule organization has a subtle but detectable effect on the membrane organization of MHC I. Finally, a decrease of temperature at 25° leads to a global decrease of ψ-values by 5–10°.

Orientational order behavior of di-8-ANEPPQ

To address the question of the orientational order of lipid molecules in cell membranes and its possible correlation with the MHC I behavior, di-8-ANEPPQ was incorporated into the COS-7 cell membranes. Di-8-ANEPPQ exhibits a transition dipole within the membrane leaflets and therefore is expected to qualitatively report the local lipid order (19). As a consequence, the orientational order behavior of di-8-ANEPPQ is expected to give a relevant indication on the MHC I surrounding lipid environment. Only the plasma membrane is probed in this case because the insertion of the di-8-ANEPPQ occurs mainly within this membrane and is stopped before the probe reaching the cytosol. The absorption and emission dipoles of di-8-ANEPPQ are supposed to lie along roughly the same direction, based on demonstrations performed on TMA-DPH, which is a similar one-dimensional molecule (30). Fig. 2 shows the anisotropy images of di-8-ANEPPQ inserted into COS-7 cells for different cell treatments. In untreated cells, a high anisotropy value is observed for the lipid probe, signature of a higher orientational order ($\psi = 132° \pm 12°$) than the one observed for MHC^{GFP}Rigid. Cell swelling by a hypotonic shock leads to a strong increase of orientational order with $\psi = 98° \pm 10°$. Treatments altering the actin cytoskeleton network cause similar effects but slightly less pronounced with a cone aperture angle ψ of ($116° \pm 10°$) for latrunculin A and $\psi = 108° \pm 12°$ for cytochalasin D. Similarly, the colcemid treatment also increases the orientational order of di-8-ANEPPQ with a cone aperture angle ψ of ($117° \pm 11°$). These results are summarized in Table 1. At last, a temperature decrease down to 25° leads to a decrease of the cone apertures by 10–20° (see the Supporting Material).

DISCUSSION

In this study, the GFP molecule attached to the MHC^{GFP}Rigid construct is considered to be a relevant reporter of the MHC I orientational order changes in the membranes upon drug effects, whereas the di-8-ANEPPQ molecules are reporter for the surrounding membrane lipid order. Although these fluorophores give a partial view of the orientation of both MHC I and lipids, because they are not rigidly parallel to the proteins and lipids molecules, they are able to report the sensitivity of these molecules (in terms of order and disorder changes) relative to cell treatments. In particular, we probed the modification on the orientational order of lipids and proteins in the plasma membrane after the disruption of actin cytoskeleton and the microtubule network. Note that the orientational order probed in this work is a steady-state quantity, because orientational fluctuations occur at a much faster timescale than the measurement time used. Although this fast orientational dynamics is known for lipid probes (14), we confirmed this assumption by polarized fluorescence correlation spectroscopy measurements on MHC^{GFP}Rigid and MHC^{GFP}Flexible in cell membranes (see the Supporting Material).

Sensitivity of the molecular order ψ determination

The $A(\psi)$ dependence presented in Fig. 1 *e* for $\rho = 0°$ shows that the technique is highly sensitive to a small change in the cone aperture ψ of the molecular orientation distribution especially around high cones apertures. A decrease of sensitivity could be expected from a poor signal/noise ratio and a large heterogeneity of behaviors in the explored population. In the our case, the detected intensity was high enough to provide a signal/noise ratio over 16 for di-8-ANEPPQ probe and 11 for the MHC^{GFP}Rigid probe, which is sufficient to obtain a reliability of a few percent in the determination of the anisotropy ratio A, and therefore of a few degrees for ψ. Furthermore, the histograms of measured angles ψ over 200 areas in the cells show a homogeneous behavior (Fig. 3). Increasing the statistics to 1000 regions of interest does not change significantly the shape of this histogram or the mean value of ψ. In addition, several repeated measurements over the same cell give the same result for the mean ψ with a few degrees precision. The width observed on the ψ-histograms (resulting from a standard deviation of A of ~0.04–0.08) is therefore instead assigned to the heterogeneity of the local environment around the cell membranes contour, and from one cell to another. Therefore, we consider that the histogram relative displacements observed for different cells conditions (Fig. 3) accurately relate to specific molecular organization of the probed component within biomembranes.

We have been able to rule out the major different physical possibilities that might contribute to a misleading estimation of ψ.

First, all instrumental polarization mixture factors such as excitation polarization distortions and high numerical aperture collection are accounted for in the analysis, and can be ruled out in the possible error sources.

Second, the hypothesis of parallel absorption/emission dipoles is supported by previous measurements (12,30).

Third, the supposition of a perfect cone orientation in the (X,Y) plane has been tested by a separate measurement of the cell profiles, which shows that in the measured cell

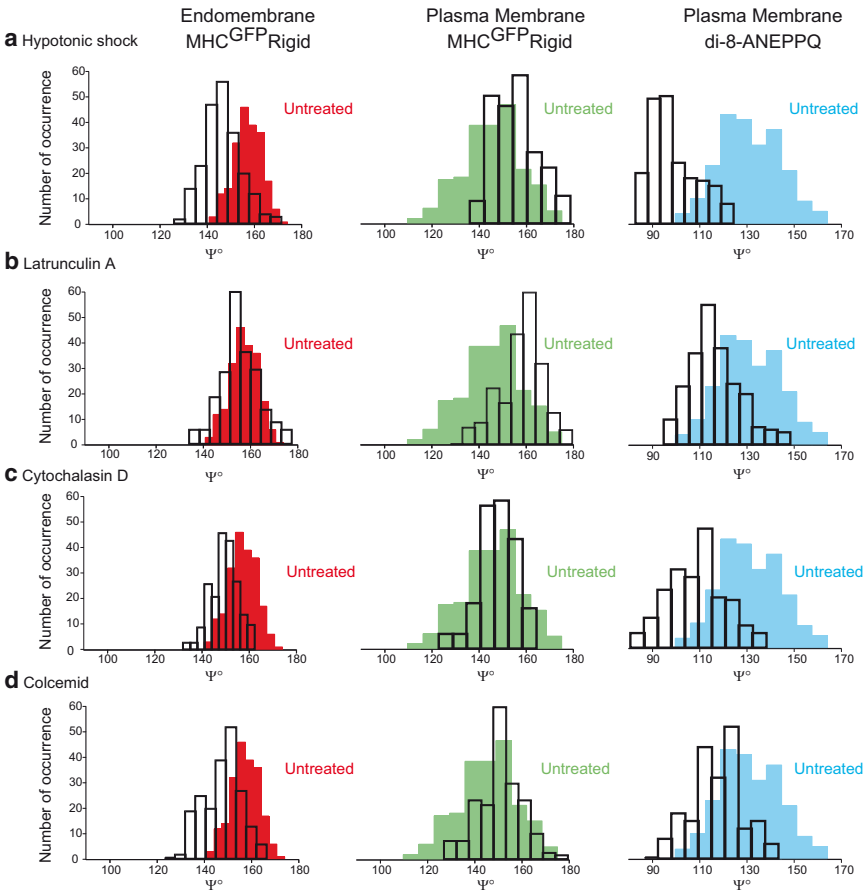

FIGURE 3 Histograms showing the cone aperture angle distribution ψ before (*plain histograms*) and after the treatments (*line histograms*) with (*a*) hypotonic shock, (*b*) latrunculin A, (*c*) cytochalasin D, and (*d*) colcemid, for MHC^{GFP}Rigid in both the endomembrane (*left*) and the plasma membrane (*middle*), and di-8-ANEPPQ in the plasma membrane (*right*). All measurements are performed at 37°C. In each case, the statistics are performed on 200 total areas taken within a population of 5–10 cells.

equator the off-plane orientation is small enough (<20°) to support this hypothesis (19).

Fourth, an overestimation of the cone aperture ψ might result from Förster resonant energy transfer between adjacent fluorescent probes (homo-FRET). Indeed energy transfer can lead to a depolarization of the measured fluorescent signal and therefore to an artificial enlargement of the observed distribution. Homo-FRET is usually employed as a signature of the presence of proteins dimerization or aggregation (31,32). In the case of MHC I, homo-FRET has been evidenced by an anisotropy decrease in the endomembrane, which was interpreted as a more pronounced clustering of MHC I that was not observed in matured proteins (12). Clustering of peptide-loaded MHC I proteins have also been observed, indicating the role of aggregation in T cell recognition processes (3,4). In the plasma membrane, the MHC proteins are matured and the most informative data are obtained there.

To probe possible homo-FRET between MHC proteins or di-8-ANEPPQ lipid probes, we have performed a successive bleaching experiment, at long timescales (10–20 min) of continuous illumination. When performing anisotropy measurements after progressive decrease of the number of fluorescent molecules due to photobleaching, the anisotropy is expected to decrease if there is significant homo-FRET between molecules. This effect is not observed for either MHC I in both membranes or di- 8-ANEPPQ (see the Supporting Material). Note, however, that a small degree of homo-FRET for MHC^{GFP}Rigid in the endomembrane might be probable due to the higher protein concentration and possible clustering of the proteins in the endoplasmic reticulum (12,22). A remaining homo-FRET effect not measurable with our sensitivity would not affect the comparisons between the different cells treatments, though, which are relative analyses based on the same concentration conditions.

Analysis of MHC I and lipid probes orientational order

The MHC^{GFP}Rigid protein label exhibits the required properties to be a reporter for the protein orientational order in the membrane, due to the restriction of its orientational degrees of freedom in the nuclear and the plasma membrane. In contrast, MHC^{GFP}Flexible shows a completely isotropic behavior (Fig. 2, *b* and *e*) due to the fact that GFP is labeled at the protein C-terminus in a flexible way and is allowed to explore all possible orientation angles. Nevertheless, the measured ψ-aperture angle for MHC^{GFP}Rigid is still quite high (between 140° and 160°, Table 1), which shows either that GFP is still not completely

rigidly attached to the construct, or that the construct undergoes itself some degree of orientation disorder in the membrane. Nevertheless, the MHC^{GFP}Rigid disorder being lower than an isotropic behavior of MHC^{GFP}Flexible can be considered as a reference point for relative comparisons among the endomembrane and the plasma membrane, different temperature conditions, and cell treatments effects.

Our results show that MHC^{GFP}Rigid in the untreated plasma membrane exhibits a higher orientational order than in the endomembrane (Table 1). We explain this observation with the fact that:

First, the endomembrane exhibits a more complex multilayer structure with a higher proficiency to induce a disorder into the proteins orientation.

Second, the proteins in the nuclear membrane are not completely matured, allowing different orientations of the GFP.

Third, the different composition of the lipids in the two membranes indicates a higher presence of orienting lipid molecules in the plasma membrane, leading to a higher order of the proteins.

Fourth, a possible degree of homo-FRET in the endomembrane might lead to an enlargement of the measured aperture angle in this region, as mentioned above.

If existing, this transfer is, however, not complete because a change of ψ in the endomembrane has been observed under some cell treatments and change of temperature. In particular in the two membranes, the molecular disorder is seen to increase when increasing the temperature from 25°C to 37°C (see the Supporting Material), which is consistent with a higher thermal agitation.

These results show overall slightly larger ψ-angles than previously measured on the same proteins constructs (12), where $\psi \sim 100^\circ$ was found in MHC^{GFP}Rigid. This measurement was performed on cell blebs, though, which can affect the cell by a strong structural change. In our work, fluorescence polarization-resolved imaging has been performed on unperturbed living cells in which both endomembrane and plasma membrane can be separately visualized.

The di-8-ANEPPQ molecule is a good reporter for the orientational order of lipid molecules even though the labeling is restricted to the plasma membrane. An adequate exposure time of the cells into the di-8-ANEPPQ insertion buffer permits us to achieve a well-contrasted fluorescence signal between the plasma membrane and its surrounding (interior and exterior of the cells), without reaching a too-high concentration which would lead to homo-FRET depolarization effects. We find a higher order of the di-8-ANEPPQ fluorophores in the plasma membrane, as compared to MHC I. This result is consistent with the deeper incorporation of the lipid probe within the plasma membrane in contrast to the MHC^{GFP}Rigid where the GFP is located outside of the plasma membrane, therefore undergoing less constraining orientational potential. It is important to point out that comparison of the ψ-aperture angle observed for different molecules should integrate this initial degree of steric constraint.

The measured lipid probe orientational order is comparable with measurements obtained in liquid-disordered phases of giant unilamellar vesicles at the same temperature conditions (19). This result is therefore representative of a disordered environment rather than a constrained one. This is most likely to occur because of the averaging specificity of the imaging technique: all orientational information is indeed averaged over long times (100 μs) comparing to the lipids rotational diffusion times (see the Supporting Material), and over large spatial scales (200 nm) comparing to the lipids and membrane microscopic features sizes. In particular, there are some evidences that cell membranes are not totally flat but instead made of subresolution scales wrinkles (2,5,33,34). It is therefore expected that averaging over this membrane complex and dynamical boundary would result in quite large cone aperture angles.

Nevertheless, even though the measured cone aperture ψ for lipid probes contains structural wrinkles averaging, it is still sensitive to membrane treatments and temperature. In particular, at a physiological temperature (37°C), the di-8-ANEPPQ fluorophores exhibit a higher disorder due to larger thermal fluctuations. This indicates that both morphology effects and environment dynamics are responsible for the observed molecular orientational order.

Treatments effects on the orientational order of MHC I and the lipid probes

We probed the effect of actin-based and microtubule-based cytoskeleton network perturbation on the molecular order of MHC I in both endomembrane and plasma membranes, as well as the di-8-ANEPPQ lipid probe order in the plasma membrane. Latrunculin A associates only with actin monomers, preventing them from their repolymerization into filaments. We observe that the treatment with latrunculin A does not affect the MHC^{GFP}Rigid molecule orientational order in the endomembrane, but there is a clear effect on disorder of the protein in the plasma membrane with an increase of the ψ-angle by $>10^\circ$ (Table 1). The plasma membrane is connected to the cytoskeleton via transmembrane proteins, and disrupting this network visibly induces a disorder in the membrane proteins. The order observed in cells without any treatment is therefore due to the cytoskeleton binding network—which thus contributes to the proteins orientational stability. This is expected for membrane proteins which are strongly interacting with the underlying cytoskeleton (4), leading to important consequences on their biological function (35–37). MHC I in the endomembrane, on the contrary, is less affected by latrunculin A, which diffuses toward the interior of the cell with less efficiency.

The effect of hypotonic shock on MHC I in the plasma membrane follows roughly the same trends as for latrunculin A, which supports the indication that direct or indirect relation with the cytoskeleton affects MHC I orientational order. The cell swelling, however, exhibits a more pronounced effect on the endomembrane proteins for which an order is induced, which could be due to an indirect relation between perturbation of the cytoskeleton filaments network and the endomembrane structure (38). In the case of cytochalasin D, which provides weaker effect than latrunculin A, the plasma membrane proteins are seen to be almost unaffected, whereas the endomembrane follows again the same trend as for cells swelling. Colcemid finally induces a slight disorder in the plasma membrane, and again a higher order in the endomembrane. Overall, the results show that the orientational order of MHC I is, to some extent, perturbed by its interaction with the cytoskeleton: the general trend being an increased disorder in the plasma membrane and a slightly increased order in the endomembrane.

The first effect could be related to a decreased interaction with the cytoskeleton, the second one with an indirect consequence of the cell treatments on the endomembrane.

The di-8-ANEPPQ molecules in the plasma membrane exhibit a very different behavior, with an increase of the orientational order after disruption of the actin cytoskeleton and microtubule network. A possible explanation for this observation is that after the loss of its link to the cytoskeleton, the plasma membrane experiences a higher tension, leading to less prominent morphological subwavelength features, and therefore a higher order in a smaller cone aperture angles ψ. Fig. 4 summarizes the results obtained for the untreated cells compared to latrunculin A treatment in a schematic representation.

CONCLUSION

In this work we have shown that one photon fluorescence anisotropy imaging, completed with fully polarization resolved measurements, is sensitive enough to detect small changes in the orientational order of proteins and lipids in cell membranes with respect to temperature changes as well as actin cytoskeleton and microtubule networks alterations. We found that the cytoskeleton links with the plasma membrane and the MHC I protein plays an important role on their respective orientation, with a more or less pronounced effect depending on the treatment used. When disrupting the cytoskeleton network with latrunculin A or an hypotonic shock, MHC I is in particular more disordered due to missing connection with actin filaments. On the contrary, the lipid reporter di-8-ANEPPQs turn out to be more ordered most probably due to increased local membrane tension. These results show that orientational order investigations can potentially be further related to the biological functions of molecules in which there is a strong interplay between nanometric scales interactions and orientational effects.

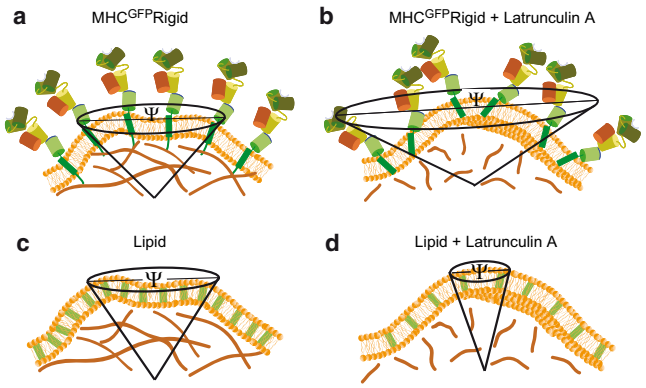

FIGURE 4 Proposed scheme for (*a*) MHC I and (*c*) di-8-ANEPPQ orientational behavior in the untreated case and (*b*) MHC I and (*d*) di-8-ANEPPQ after actin polymerization inhibition with Latrunculin A.

SUPPORTING MATERIAL

Additional information with eight figures and one table is available at http://www.biophysj.org/biophysj/supplemental/S0006-3495(11)00591-1.

We thank S. Mailfert from Centre d'Immunologie de Marseille Luminy, France, for help with the FCS data treatment as well as P. Schön, H. Ranchon and W. Wang from Institut Fresnel, MOSAIC, for help with data analysis programming. We thank J. Savatier from Institut Fresnel, MOSAIC, for advice in cell treatment.

This work is partly supported by the Provence-Alpes-Côte d'Azur region, France. This work is supported by the Agence Nationale de la Recherche, grants Nos. ANR 2010 BLAN 150902 (ReceptORIENT) and 121402 (NanoDIGICODE). S.B., P.F., and H.R. are supported by grants from CNRS. T.T., H.T.H., and D.M. are supported by institutional grants from INSERM and CNRS, and by grants from the Institut National du Cancer, the Fondation pour la Recherche Médicale.

REFERENCES

1. Heresh, D., J. Leng, and R. Klemke. 1999. Regulation of cell contraction and membrane ruffling by distinct signals in migratory cells. *J. Cell Biol.* 146:1107–1116.
2. Anantharam, A., B. Onoa, …, D. Axelrod. 2010. Localized topological changes of the plasma membrane upon exocytosis visualized by polarized TIRFM. *J. Cell Biol.* 188:415–428.
3. Pentcheva, T., and M. Edidin. 2001. Clustering of peptide-loaded MHC class I molecules for endoplasmic reticulum export imaged by fluorescence resonance energy transfer. *J. Immunol.* 166:6625–6632.
4. Fooksman, D. R., G. K. Grönvall, …, M. Edidin. 2006. Clustering class I MHC modulates sensitivity of T cell recognition. *J. Immunol.* 176: 6673–6680.
5. Benninger, R. K. P., B. Vanherberghen, …, B. Onfelt. 2009. Live cell linear dichroism imaging reveals extensive membrane ruffling within the docking structure of natural killer cell immune synapses. *Biophys. J.* 96:L13–L15.
6. Borejdo, J., and S. Burlacu. 1993. Measuring orientation of actin filaments within a cell: orientation of actin in intestinal microvilli. *Biophys. J.* 65:300–309.
7. Brack, A. S., B. D. Brandmeier, …, M. Irving. 2004. Bifunctional rhodamine probes of Myosin regulatory light chain orientation in relaxed skeletal muscle fibers. *Biophys. J.* 86:2329–2341.
8. Vrabioiu, A. M., and T. J. Mitchison. 2006. Structural insights into yeast septin organization from polarized fluorescence microscopy. *Nature.* 443:466–469.

9. Schlessinger, J., D. E. Koppel, …, E. L. Elson. 1976. Lateral transport on cell membranes: mobility of concanavalin A receptors on myoblasts. *Proc. Natl. Acad. Sci. USA*. 73:2409–2413.
10. Schwille, P., U. Haupts, …, W. W. Webb. 1999. Molecular dynamics in living cells observed by fluorescence correlation spectroscopy with one- and two-photon excitation. *Biophys. J.* 77:2251–2265.
11. Schütz, G. J., G. Kada, …, H. Schindler. 2000. Properties of lipid microdomains in a muscle cell membrane visualized by single molecule microscopy. *EMBO J.* 19:892–901.
12. Rocheleau, J. V., M. Edidin, and D. W. Piston. 2003. Intrasequence GFP in class I MHC molecules, a rigid probe for fluorescence anisotropy measurements of the membrane environment. *Biophys. J.* 84: 4078–4086.
13. Axelrod, D. 1979. Carbocyanine dye orientation in red cell membrane studied by microscopic fluorescence polarization. *Biophys. J.* 26: 557–573.
14. Florine-Casteel, K. 1990. Phospholipid order in gel- and fluid-phase cell-size liposomes measured by digitized video fluorescence polarization microscopy. *Biophys. J.* 57:1199–1215.
15. Blackman, S. M., C. E. Cobb, …, D. W. Piston. 1996. The orientation of eosin-5-maleimide on human erythrocyte band 3 measured by fluorescence polarization microscopy. *Biophys. J.* 71:194–208.
16. Gidwani, A., D. Holowka, and B. Baird. 2001. Fluorescence anisotropy measurements of lipid order in plasma membranes and lipid rafts from RBL-2H3 mast cells. *Biochemistry.* 40:12422–12429.
17. Benninger, R. K. P., B. Önfelt, …, P. M. French. 2005. Fluorescence imaging of two-photon linear dichroism: cholesterol depletion disrupts molecular orientation in cell membranes. *Biophys. J.* 88:609–622.
18. Dale, R. E., S. C. Hopkins, …, Y. E. Goldman. 1999. Model-independent analysis of the orientation of fluorescent probes with restricted mobility in muscle fibers. *Biophys. J.* 76:1606–1618.
19. Gasecka, A., T.-J. Han, …, S. Brasselet. 2009. Quantitative imaging of molecular order in lipid membranes using two-photon fluorescence polarimetry. *Biophys. J.* 97:2854–2862.
20. Haluska, C. K., A. P. Schröder, …, C. M. Marques. 2008. Combining fluorescence lifetime and polarization microscopy to discriminate phase separated domains in giant unilamellar vesicles. *Biophys. J.* 95: 5737–5747.
21. Mattheyses, A. L., M. Kampmann, …, S. M. Simon. 2010. Fluorescence anisotropy reveals order and disorder of protein domains in the nuclear pore complex. *Biophys. J.* 99:1706–1717.
22. Marguet, D., E. T. Spiliotis, …, M. Edidin. 1999. Lateral diffusion of GFP-tagged H2Ld molecules and of GFP-TAP1 reports on the assembly and retention of these molecules in the endoplasmic reticulum. *Immunity.* 11:231–240.
23. LeFloc'h, V., S. Brasselet, …, J. Zyss. 2003. Monitoring of orientation in molecular ensembles by polarization sensitive nonlinear microscopy. *J. Phys. Chem. B.* 107:12403–12410.
24. Edidin, M., S. C. Kuo, and M. P. Sheetz. 1991. Lateral movements of membrane glycoproteins restricted by dynamic cytoplasmic barriers. *Science.* 254:1379–1382.
25. Edidin, M., M. C. Zúñiga, and M. P. Sheetz. 1994. Truncation mutants define and locate cytoplasmic barriers to lateral mobility of membrane glycoproteins. *Proc. Natl. Acad. Sci. USA*. 91:3378–3382.
26. Gombos, I., E. Kiss, …, J. Matkó. 2006. Cholesterol and sphingolipids as lipid organizers of the immune cells' plasma membrane: their impact on the functions of MHC molecules, effector T-lymphocytes and T-cell death. *Immunol. Lett.* 104:59–69.
27. Ma, Z., K. A. Sharp, …, T. H. Finkel. 2008. Surface-anchored monomeric agonist pMHCs alone trigger TCR with high sensitivity. *PLoS Biol.* 6:e43.
28. Ferrand, P., M. Pianta, …, D. Marguet. 2009. A versatile dual spot laser scanning confocal microscopy system for advanced fluorescence correlation spectroscopy analysis in living cell. *Rev. Sci. Instrum.* 80:083702–083708.
29. Schön, P., F. Munhoz, …, S. Brasselet. 2008. Polarization distortion effects in polarimetric two-photon microscopy. *Opt. Express.* 16:20891–20901.
30. Muller, J. M., D. H. Harryvan, …, E. E. van Faassen. 1996. The orientation of the transition dipole moments of TMA-DPH embedded in a poly(vinylalcohol) film. *Chem. Phys.* 211:413–420.
31. Blackman, S. M., D. W. Piston, and A. H. Beth. 1998. Oligomeric state of human erythrocyte band 3 measured by fluorescence resonance energy homotransfer. *Biophys. J.* 75:1117–1130.
32. Gautier, I., M. Tramier, …, M. Coppey-Moisan. 2001. Homo-FRET microscopy in living cells to measure monomer-dimer transition of GFP-tagged proteins. *Biophys. J.* 80:3000–3008.
33. van Rheenen, J., and K. Jalink. 2002. Agonist-induced PIP(2) hydrolysis inhibits cortical actin dynamics: regulation at a global but not at a micrometer scale. *Mol. Biol. Cell.* 13:3257–3267.
34. Adler, J., A. I. Shevchuk, …, I. Parmryd. 2010. Plasma membrane topography and interpretation of single-particle tracks. *Nat. Methods.* 7:170–171.
35. Bunnell, S. C., V. Kapoor, …, L. E. Samelson. 2001. Dynamic actin polymerization drives T cell receptor-induced spreading: a role for the signal transduction adaptor LAT. *Immunity.* 14:315–329.
36. Barda-Saad, M., A. Braiman, …, L. E. Samelson. 2005. Dynamic molecular interactions linking the T cell antigen receptor to the actin cytoskeleton. *Nat. Immunol.* 6:80–89.
37. Treanor, B., D. Depoil, …, F. D. Batista. 2010. The membrane skeleton controls diffusion dynamics and signaling through the B cell receptor. *Immunity.* 32:187–199.
38. Schauer, K., T. Duong, …, B. Goud. 2010. Probabilistic density maps to study global endomembrane organization. *Nat. Methods.* 7:560–566.